International Journal of Nanomedicine

Dovepress
open access to scientific and medical research

Open Access Full Text Article

ORIGINAL RESEARCH

A Unique Approach: Biomimetic Graphdiyne-Based Nanoplatform to Treat Prostate Cancer by Combining Cuproptosis and Enhanced Chemodynamic Therapy

Wenjie Xie[1,2,*], Yixun Zhang[1,2,*], Qianfeng Xu[1,2,*], Guowei Zhong[1,2], Jundong Lin[2,3], Huichan He[3], Qiuling Du[2], Huijing Tan[1,2], Muqi Chen[1,2], Zhenjie Wu[1–3], Yulin Deng[1,2], Zhaodong Han[1–3], Jianming Lu[1,2,4], Jianheng Ye[1,2,4], Fen Zou[1,2], Yangjia Zhuo[1,2], Weide Zhong[1–4]

[1]Department of Urology, The Second Affiliated Hospital, School of Medicine, South China University of Technology, Guangzhou, 510180, People's Republic of China; [2]Guangdong Key Laboratory of Clinical Molecular Medicine and Diagnostics, Guangzhou First People's Hospital, School of Medicine, South China University of Technology, Guangzhou, 510180, People's Republic of China; [3]Urology Key Laboratory of Guangdong Province, The First Affiliated Hospital of Guangzhou Medical University, Guangzhou, 510230, People's Republic of China; [4]State Key Laboratory of Quality Research in Chinese Medicine, Macau University of Science and Technology, Taipa, Macau, 999078, People's Republic of China

*These authors contributed equally to this work

Correspondence: Yangjia Zhuo; WeideZhong, Email eyyangjiazhuo@scut.edu.cn; zhongwd2009@live.cn

Purpose: Current treatment approaches for Prostate cancer (PCa) often come with debilitating side effects and limited therapeutic outcomes. There is urgent need for an alternative effective and safe treatment for PCa.

Methods: We developed a nanoplatform to target prostate cancer cells based on graphdiyne (GDY) and a copper-based metal-organic framework (GDY-CuMOF), that carries the chemotherapy drug doxorubicin (DOX) for cancer treatment. Moreover, to provide GDY-CuMOF@DOX with homotypic targeting capability, we coated the PCa cell membrane (DU145 cell membrane, DCM) onto the surface of GDY-CuMOF@DOX, thus obtaining a biomimetic nanoplatform (DCM@GDY-CuMOF@DOX). The nanoplatform was characterized by using transmission electron microscope, atomic force microscope, X-ray diffraction, etc. Drug release behavior, antitumor effects in vivo and in vitro, and biosafety of the nanoplatform were evaluated.

Results: We found that GDY-CuMOF exhibited a remarkable capability to load DOX mainly through π-conjugation and pore adsorption, and it responsively released DOX and generated Cu^{+} in the presence of glutathione (GSH). In vivo experiments demonstrated that this nanoplatform exhibits remarkable cell-killing efficiency by generating lethal reactive oxygen species (ROS) and mediating cuproptosis. In addition, DCM@GDY-CuMOF@DOX effectively suppresses tumor growth in vivo without causing any apparent side effects.

Conclusion: The constructed DCM@GDY-CuMOF@DOX nanoplatform integrates tumor targeting, drug-responsive release and combination with cuproptosis and chemodynamic therapy, offering insights for further biomedical research on efficient PCa treatment.

Keywords: graphdiyne, biomimetic nanoplatform, cuproptosis, chemotherapy, prostate cancer

Introduction

Prostate cancer (PCa) is caused by one of the most common malignant tumors resulting in high morbidity and mortality in males.[1] Most patients with PCa are already at an advanced stage of the tumor at the time of diagnosis.[2] Endocrine therapy with androgen deprivation is the current standard of care therapy. Although androgen deprivation therapy has beneficial effects on advanced-stage PCa, this endocrine therapy inevitably promotes the emergence of castration-resistant prostate cancer (CRPC), which can accelerate the tumor metastasis, render chemotherapy, endocrine therapy,

Received: 22 January 2024
Accepted: 20 April 2024
Published: 2 May 2024

Graphical Abstract

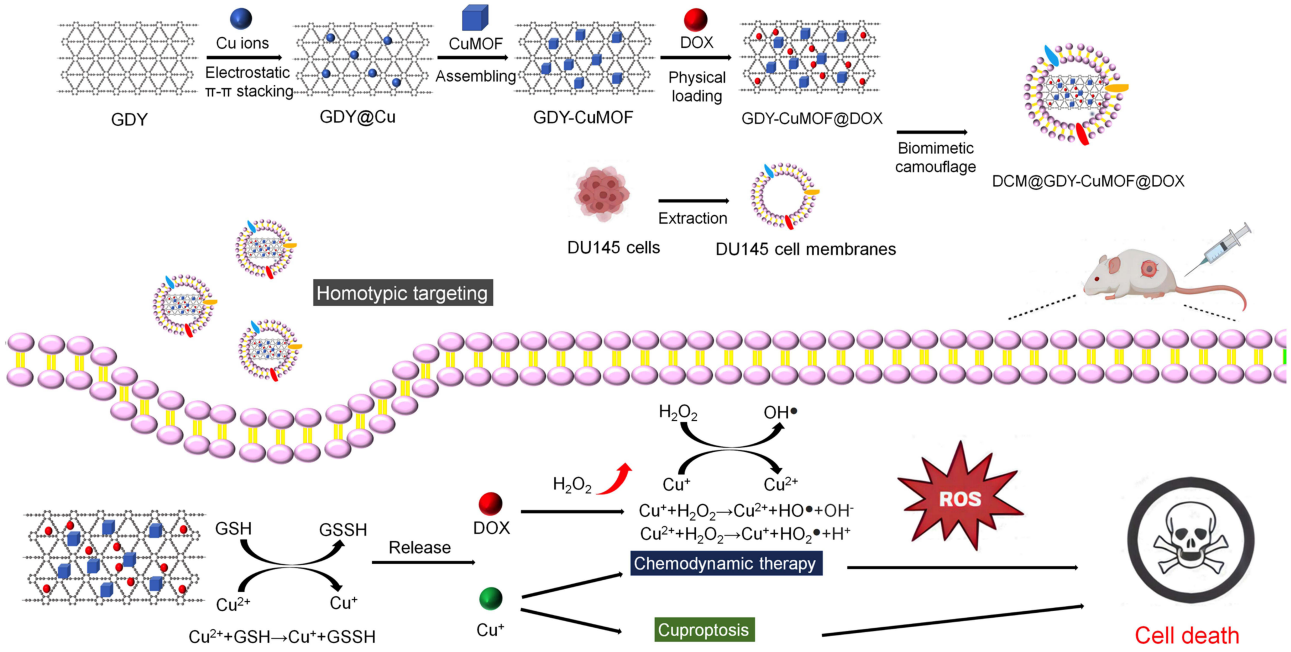

or immunotherapy ineffective and ultimately shorten patient survival time.[3–6] Considering the limitations of the clinical treatment for PCa, there is urgent need for an alternative effective and safe treatment for PCa.

Copper (Cu) is an essential trace element present in all organisms and plays a crucial role in bioactivity. In biological systems, Cu is involved in many redox reactions as a cofactor for various enzymes, shifting between two oxidation states (Cu^{2+} and Cu^{+}).[7] Bioavailable Cu serves as a structural component in many proteins and ligands.[8] Organisms maintain the concentration of Cu ions through an inherently sophisticated regulation system ensuring that free Cu ions are usually less than one atom per cell.[9] Excessive Cu levels may disrupt homeostatic mechanisms, resulting in severe systemic toxicity.[10] A recent study by Tsvetkov et al has revealed a unique copper-dependent form of nonapoptotic cell death, which they termed "cuproptosis".[11] Cuproptosis, a novel form of programmed cell death, is characterized by the binding of excess intracellular copper to lipoylated proteins in tricarboxylic acid (TCA) cycle. This process leads to the aggregation of lipoylated proteins and loss of iron-sulfur (Fe-S) cluster proteins, ultimately resulting in cell death. Unlike known cell death pathways, such as apoptosis, necroptosis, pyroptosis, and ferroptosis, cuproptosis depend on the accumulation of intracellular copper and mitochondrial respiration.[12] Given that energy production in aggressive PCa cells is primarily through the TCA cycle,[13] we expected that the programmed cell death induced by cuproptosis, which interferes with the TCA cycle, may provide some insights for PCa treatment.

Inspired by the unique mechanism of cuproptosis, the rational design of efficacious tumor therapeutic strategies based on cuproptosis has attracted growing attention. However, the concentration of Cu ions in tumor cells is too low to achieve this therapeutic strategy.[14] Moreover, it may cause severe toxicity through the non-selective accumulation of copper in normal regions owing to the untargeted property of copper delivery.[15] Hence, to avoid excessive generation of free copper ions in the circulation, it is essential to develop a cuproptosis-based therapy to spatiotemporally confine copper ions within tumor cells.[16] In recent years, a novel two-dimensional (2D) all-carbon material, graphdiyne (GDY), with a conjugated network of sp^2-hybridized carbon atoms from benzene rings and sp-hybridized carbon atoms from acetylene units was proposed as a target support for anchoring and immobilizing metal molecules.[17–21] Compared with the traditional sp^2-hybridized carbon materials, the 2D morphological structure of GDY possesses numerous macropores,

high π-conjugation, and an excellent specific surface, making it more suitable for constructing an efficient metallic molecular delivery system.

Doxorubicin (DOX) is the most commonly used anthracycline for cancer chemotherapy. DOX can generate a large amount of H_2O_2, which can be converted into lethal reactive oxygen species (ROS) through a Fenton-like reaction, involving a valence shift from Cu^+ to Cu^{2+}. This process results in efficient chemodynamic therapy.[22–26] Considering that the toxicity associated with cuproptosis is mainly linked to Cu^+, the combination of cuproptosis-based therapy and enhanced chemodynamic therapy involving DOX is expected to hold potential for PCa treatment. Along these lines, we tailored the GDY substrate with a copper-based metal-organic framework (GDY-CuMOF), featuring a coordinated network formed by inorganic copper ions connected to organic 1.4-benzenedicarboxylate (H_2BDC) nodes immobilized onto the GDY surface, and loaded DOX onto the copper-containing nanomaterial (GDY-CuMOF@DOX). Furthermore, to provide GDY-CuMOF@DOX with homotypic targeting capability, we coated the PCa cell membrane (DU145 cell membrane, DCM) onto the surface of GDY-CuMOF@DOX, thus obtaining a biomimetic nanoplatform (DCM@GDY-CuMOF@DOX). Surprisingly, we found that GDY-CuMOF exhibited a remarkable capability to load DOX mainly through π-conjugation and pore adsorption, and it responsively released DOX and generated Cu^+ in the presence of glutathione (GSH). In vivo experiments demonstrated that DCM@GDY-CuMOF@DOX efficiently accumulated in PCa cells, benefiting from homologous cells camouflage, and inducing a high level of intracellular ROS production. A more in-depth investigation of the antitumor mechanism of DCM@GDY-CuMOF@DOX revealed that this Cu-containing nanoplatform killed PCa cells by inducing ROS and mediating cuproptosis. In vivo experiments confirmed the anticancer efficacy of DCM@GDY-CuMOF@DOX. In summary, DCM@GDY-CuMOF@DOX can serve as a selective, effective, and safe therapeutic nanomaterial for PCa treatment.

Materials and Methods

Materials

Tetrahydrofuran (THF), anhydrous sodium sulfate (Na_2SO_4), N,N-Dimethylformamide (DMF), copper nitrate trihydrate ($Cu(NO_3)_2{\cdot}3H_2O$), and *p*-phthalic acid (H_2BDC) were procured from Aladdin (Shanghai, China). Tetrabutylammonium fluoride (TBAF) was purchased from Beijing InnoChem Science and Technology Co., Ltd. Polyvinylpyrrolidone (PVP) and doxorubicin hydrochloride (DOX) were procured from Shanghai Yuanye Biotechnology Co., Ltd. Roswell Park Memorial Institute (RPMI) 1640 medium, fetal bovine serum (FBS), penicillin-streptomycin and phosphate-buffered saline (PBS) were purchased from Gibco (USA). The cell counting Kit-8 (CCK-8) was obtained from Meilunbio (Dalian, China). The ROS assay kit was procured from Beyotime Biotechnology (Shanghai, China). Unless otherwise stated, all the solvents and chemicals were purchased commercially and used without further purification.

Synthesis of GDY

GDY was synthesized following a previously published report.[27] In brief, the hexakis[(trimethylsilyl) ethynyl]-benzene monomer (HEB-TMS) and TBAF were combined in THF, and the mixture was stirred at 0 °C for 10 min. The resulting solution was then diluted with ethyl acetate, and washed with brine and dried over anhydrous Na_2SO_4. Subsequently, the solvent was removed under vacuum to yield the deprotected hexaethynylbenzene (HEB) monomer.

The reactants were further diluted with pyridine and slowly introduced to a Cu foil in pyridine solution under a nitrogen atmosphere at 110 °C for 72 h. Cu foils loaded with GDY were dissolved in hot acetone and hot DMF followed by sonication for 1 h. The resulting black solid was refluxed overnight at 80 °C in a 2 M sodium hydroxide solution, 2 M hydrochloric acid solution and another 2 M sodium hydroxide solution, respectively. Subsequently, the product was washed multiple times with ultrapure water and acetone, and collected via centrifugation, and dried to obtain pure GDY nanosheets.

Synthesis of GDY-CuMOF

First, 5 mg of GDY nanosheets and 52 mg of $Cu(NO_3)_2{\cdot}3H_2O$ were dissolved in an aqueous solution. $Cu(NO_3)_2$ was then loaded onto the surface of the GDY nanosheets under negative vacuum pressure to prepare GDY@Cu. Subsequently,

6 mg of PVP and GDY@Cu and 17 mg of H_2BDC were dissolved in 8 mL of DMF. The solution was stirred at room temperature for 20 min, transferred to a Teflon-lined stainless-steel autoclave and heated at 120 °C for 8 h to obtain GDY-CuMOF.

In vitro DOX Loading and Release

DOX and GDY-CuMOF were mixed in PBS (pH 7.4) at various feeding ratios (0.25, 0.5, 1, 2, 4), and stirred overnight at room temperature shielded from light. Subsequently, the DOX-loaded GDY-CuMOF (GDY-CuMOF@DOX) was gathered by centrifugation and washed three times with ultrapure water. The DOX loading content and entrapment efficiency of GDY-CuMOF@DOX were calculated using the following formulas: loading content = (weight of DOX loaded in GDY-CuMOF@DOX) / (weight of GDY-CuMOF@DOX), entrapment efficiency = (weight of DOX loaded in GDY-CuMOF@DOX) / (original weight of DOX).

For GSH-triggered DOX release, GDY-CuMOF@DOX was dissolved in PBS with or without GSH (10 mM) at two different pH levels (5.0 or 7.4) and stirred at 37 °C in the dark. The appropriate amount of supernatant was collected by centrifuging the solution at different time point. Subsequently, the concentration of DOX released into the supernatant was determined by using UV-Vis spectrometry (Shimadzu UV2600).

Extraction of DU145 Cell Membrane

DU145 cells were cultured in RPMI 1640 medium with 10% FBS and 1% penicillin-streptomycin. They were incubated in an incubator containing 5% carbon dioxide (CO_2) at 37 °C. The cells were harvested by scraping and centrifugation at 1200 rpm. Subsequently, the cells were washed three times with PBS (pH 7.4, 4 °C) and treated with a membrane extraction reagent containing 1 mM phenylmethylsulfonyl fluoride (PMSF). This mixture was placed in an ice bath for 15 min and then centrifuged at 3000 rpm for 10 min. DU145 cell membrane (DCM) was collected by centrifuging the supernatant at 14,000 rpm at 4°C and stored at −80 °C for further use.

Synthesis of DCM@GDY-CuMOF@DOX

The GDY-CuMOF@DOX solution (1 mL, 0.5 mg/mL) was introduced into a DCM solution (1 mL, 0.5 mg/mL), and ultrasonicated for 15 min to coat of the DCM. The combined solution was subsequently centrifuged at 10,000 rpm for 10 min and washed three times with ultrapure water to eliminate the free membrane. Finally, the resulting DCM@GDY-CuMOF@DOX was resuspended in PBS.

Characterization of nanomaterials

The morphological structures of GDY, GDY-CuMOF, and DCM@GDY-CuMOF@DOX were obtained using a transmission electron microscope (TEM, Talos). The phases of GDY, CuMOF, and GDY-CuMOF were analyzed by X-ray diffraction (XRD, Empyrean). The elemental mapping of GDY-CuMOF was obtained using a high-resolution TEM (HRTEM, Talos). The surface features and heights of the nanomaterials were recorded using atomic force microscopy (AFM, Bruker). The elemental compositions and valences of the nanomaterials were determined using X-ray photoelectron spectroscopy (XPS, ThermoFisher). The size and zeta potentials of GDY, GDY-CuMOF, GDY-CuMOF@DOX, and DCM@GDY-CuMOF@DOX were confirmed using a Nano Zetasizer instrument (Malvern Instruments Ltd.). The determination of the structural integrity and elemental copper composition of GDY-CuMOF after the reaction with GSH involved treating GDY-CuMOF with 10 mM GSH for 1 h. The residue was gathered by centrifugation and washed several times with ultrapure water. The height of surface features and copper composition of the residue were determined by AFM and XPS, respectively.

Sodium Dodecyl Sulfate-Polyacrylamide Gel Electrophoresis (SDS-PAGE) Protein Analysis of Nanomaterials

GDY-CuMOF@DOX and DCM@GDY-CuMOF@DOX, and DU145 cell membrane were dissolved in SDS sample buffer. The samples were heated to 100 °C for 3 minutes. Then, 20 μL of sample was loaded into each well which contained 10% SDS polyacrylamide gel. Finally, the gel was stained with Coomassie blue.

Cell Culture

DU145 cells and PC3 cells were obtained from the American Type Culture Collection. The cells were cultured in RPMI 1640 medium containing 10% FBS and 1% penicillin-streptomycin at 37 °C under 5% CO_2.

CCK-8 Assay

The effect of various nanomaterials on cell viability was evaluated using the CCK-8 assay. DU145 cells or PC3 cells were seeded in 96-well plate at a density of 1×10^3 cells/well and cultured for 24 h before the experiment. Subsequently, they were treated with various nanomaterials for 24 h and 48 h. The CCK-8 assay was carried out following to the manufacturer's instructions.

Live Cell Staining

DU145 cells were seeded in 6-well plates at a density of 3×10^5 cells/well. The cells were treated with PBS, GDY-CuMOF@DOX (10μg/mL), or DCM@GDY-CuMOF@DOX (20 μg/mL) for 24 h. Following the incubation period, the cells were washed with PBS, stained with calcein AM (2 μM) for 30 min. The images were obtained using an inverted fluorescence microscope (Olympus, Japan).

Clonogenic Assay

DU145 cells were seeded in 6-well plate at a density of 3×10^3 cells/well. The cells were treated with PBS, GDY-CuMOF@DOX (5 μg/mL), or DCM@GDY-CuMOF@DOX (5 μg/mL) for 24 h. Subsequently, the cells were incubated for 14 days, with the medium being refreshed every 2 days. Following the incubation period, the DU145 cells were gently rinsed three times with PBS, fixed with methanol for 20 min, and stained with crystal violet for 20 min. The numbers of clonogenic cells were determined using an optical microscope (Olympus Optical, Tokyo, Japan).

Wound-Healing Assay

Cell migration was assessed using a wound-healing assay. DU145 cells were seeded into 6-well plates. When the cell confluence reached approximately 80% on the plates, straight scratches were created using sterile tips. The, the medium was subsequently replaced with a serum-free medium containing PBS, GDY-CuMOF@DOX (5 μg/mL), or DCM@GDY-CuMOF@DOX (5 μg/mL) for 24 h. The scratched cultures was observed under a microscope.

Transwell Assay

Transwell assays were conducted to assess cell invasion. DU145 cells were cultured in serum-free medium for 10 h and placed into upper compartment of a chamber (Corning, USA). In the upper compartment, 200 μL of serum-free medium containing PBS, 5 μg/mL GDY-CuMOF@DOX, or DCM@GDY-CuMOF@DOX was added, while the lower compartment received complete medium. Subsequently, the cells were cultured in an atmosphere with 5% CO_2 at 37 °C for 24 h. Following incubation, the cells remaining in the upper compartment were removed, and the remaining cells were treated with 4% paraformaldehyde, and then crystal violet in sequence. Images were captured using an optical microscope.

Cellular Uptake

The cellular uptake of nanomaterials was assessed by detecting of DOX fluorescence. DU145 cells were cultured in confocal dishes. Once the cells had reached a stable state of growth, they were treated with free DOX, GDY-

CuMOF@DOX, or DCM@GDY-CuMOF@DOX with DOX at a concentration of 10 μg/mL and GDY-CuMOF@DOX and DCM@GDY-CuMOF@DOX at a concentration of 20 μg/mL for 8 h. Subsequently, the cells were rinsed three times with PBS, fixed with 4% paraformaldehyde for 1 h, and then rinsed again with PBS. DOX fluorescence was detected using the LSCM. For flow cytometry, DU145 cells were seeded in 6-well plates at a density of 5×10^5 cells/well. After 24 h of incubation, they were treated with free DOX, GDY-CuMOF@DOX, or DCM@GDY-CuMOF@DOX (equivalent DOX concentration of 10 μg/mL) for 8 h. Subsequently, the cells were rinsed three times with PBS and harvested. The DOX fluorescence in DU145 cells was determined using flow cytometry (Agilent, USA).

Cellular ROS Measurement

ROS generation in the DU145 cells was assessed using dichloro-dihydro-fluorescein diacetate (DCFH-DA) probe. DU145 cells were seeded in confocal dishes and incubated with PBS, free DOX, GDY-CuMOF@DOX, or DCM@GDY-CuMOF@DOX (DOX at 10 μg/mL, GDY-CuMOF@DOX and DCM@GDY-CuMOF@DOX at 20 μg/mL) for 24 h. Subsequently, the cells were washed with three times with PBS. Following this, the cells were treated with the fluorescent ROS probe DCFH-DA for 30 min at 37 °C. DCFH-DA fluorescence was obtained using a laser scanning confocal microscope (LSCM; Leica, Germany). In addition, DU145 were seeded in 6-well plates at a density of 3×10^5 cells/well and treated with PBS, GDY-CuMOF@DOX (10 μg/mL), or DCM@GDY-CuMOF@DOX (10 μg/mL) for 24 h. The ROS probe in cells was determined using flow cytometry.

Western Blot Assay

DU145 cells were seeded into 6-well plates. When the cell confluence reached approximately 80%, the cells were treated with PBS, GDY-CuMOF@DOX, or DCM@GDY-CuMOF@DOX at a concentration of 20 μg/mL for 24 h. Total proteins in the cells were harvested, and the expression levels of apoptosis-related proteins and cuproptosis-related proteins were assessed by a Western blot assay.

In vivo Antitumor Efficacy of DCM@GDY-CuMOF@DOX

Male BALB/c nude mice were procured from the Guangdong Medical Laboratory Animal Center for the assessment of in vivo antitumor effects. The animal experiments were performed at Guangzhou Huateng Biomedical Technology Co., Ltd. All the animal procedures were approved by the Institutional Animal Care and Use Committee of Guangzhou Huateng Biomedical Technology Co., Ltd and complied with the guidelines for the ethical review of laboratory animal welfare People's Republic of China National Standard GB/T 35892–2018. Approximately 1.0×10^6 DU145 cells were injected subcutaneously into BALB/c nude mice to establish a subcutaneous xenograft tumor model. Once the tumor volume reached 60–100 mm^3, all mice were randomly divided into four groups (n = 4), and received intravenous administrations as follows: 100 μL PBS (as control group); DOX (5 mg/kg, as positive group); GDY-CuMOF@DOX (5 mg/kg); or DCM@GDY-CuMOF@DOX (5 mg/kg) every 2 days. Different samples were injected on days 0, 3, 6, 9, and 12, totaling five injections, and the mice were observed for one week after the final injection. Tumor volume, which was calculated as length × $(width)^2$ /2 (mm^3), and tumor weight, and mouse body weight were recorded during the treatment. After the treatment period, all mice were euthanized by cervical dislocation, and tumors, along with major organs, including the heart, liver, spleen, lungs and kidney, were collected. Inductively coupled plasma mass spectrometry (ICP-MS) was conducted to detect the copper content in the tumor tissues and major organs. Hematoxylin and eosin (H&E) staining and immunohistochemical analysis of tumors was conducted to investigate the therapeutic effects of the nanoplatform. H&E staining of major organ tissues and analysis of the serum biochemical indicators were conducted to assess the biosafety of the nanoplatform.

Hemolysis Experiment

The hemolysis effect of DCM@GDY-CuMOF@DOX was evaluated using mice red blood cell suspension as previously reported.[28] Briefly, equal volumes of DCM@GDY-CuMOF@DOX suspensions were added to saline-diluted red blood cell suspension. The DCM@GDY-CuMOF@DOX concentrations were 50, 100, and 200 μg/mL, respectively. The saline was used as the negative control group and distilled water was used as the positive control group. The concentration of

the red blood cell suspension was 2.5% for all samples. All samples were incubated at 37 °C for 1.5 h. Then, the supernatant was collected and the absorbance of the supernatant at 540 nm was determined (n=5). The hemolysis ratio of DCM@GDY-CuMOF@DOX was calculated using the following formula: The hemolysis ratio = (the absorbance of the DCM@GDY-CuMOF@DOX group - The absorbance of the negative group) / (the absorbance of the positive group - The absorbance of the negative group) x 100%.

Statistical Analysis

Statistical analyses were conducted using GraphPad Prism software. The results were presented as the mean ± standard deviation (SD). Statistical analysis included one-way ANOVA and an independent sample *t*-test. Statistically significant differences were defined at $P < 0.05$.

Results and Discussion

Synthesis and Characterization of DCM@GDY-CuMOF@DOX

Initially, GDY with an average lateral dimension approximately 198 nm, were synthesized as the substrates (Figure 1A). The AFM image confirmed that the GDY exhibited a typical sheet-like morphological structure with an average height of

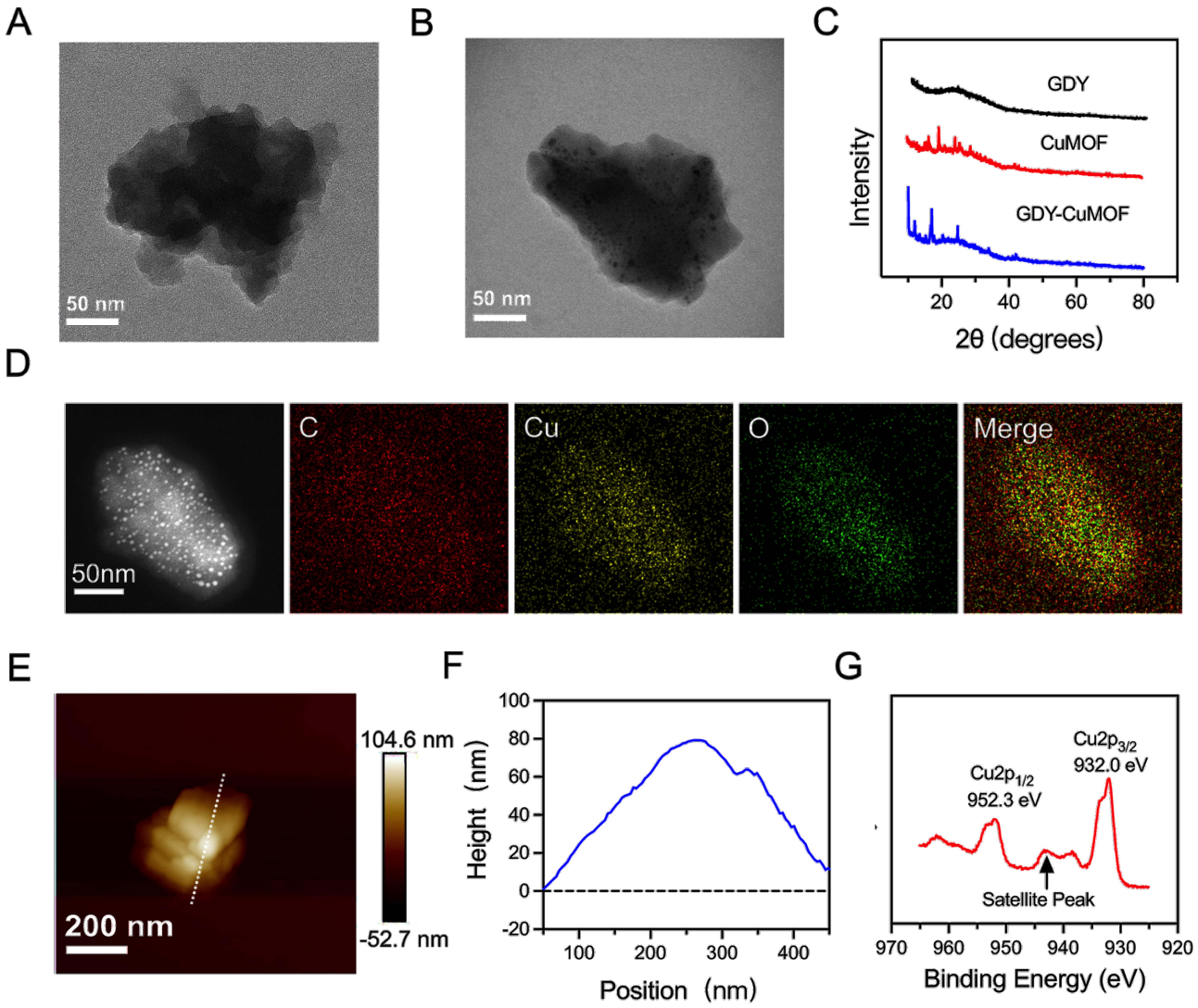

Figure 1 Characterization of GDY-CuMOF (**A**) TEM image of GDY. (**B**) TEM image of GDY-CuMOF. (**C**) XRD analysis of GDY-CuMOF. (**D**) Elemental mapping of GDY-CuMOF. (**E**) AFM image of GDY-CuMOF. (**F**) Height of GDY-CuMOF obtained from AFM. (**G**) XPS spectrum of GDY-CuMOF.

approximately 3.88 nm (Figure S1 and S2). XPS analysis indicated that carbon was the sole element present in GDY, with a binding energy of the C 1s orbital measured at 284.1 eV (Figure S3). Furthermore shown in the high-resolution asymmetric C 1s XPS of GDY displayed four characteristic subpeaks corresponding to C=C (sp^2) at 284.4 eV, C≡C (sp) at 284.9 eV, C–O at 286.2 eV, and C=O at 288.7 eV, respectively (Figure S4). This confirmed the presence of that carbon–carbon triple bonds within GDY.

Copper was linked to the GDY through cation-π interactions and electrostatic interactions. Subsequently, CuMOF was incorporated into GDY by the introduction of organic H_2BDC ligands, resulting in GDY-CuMOF. A representative TEM image revealed that GDY-CuMOF maintained the same irregular morphology as GDY (Figure 1B). The XRD pattern of GDY-CuMOF exhibited several peaks that aligned well with those of CuMOF (Figure 1C), confirming the presence of CuMOF within the GDY structure. HRTEM-EDS was utilized to further verify the elemental composition of the GDY-CuMOF. As depicted in Figure 1D, the elemental mapping results validated the composition of GDY-CuMOF and indicated the uniform distribution of the element Cu and O in the GDY substrate. Additionally, EDS revealed that the weight percentage of element Cu loaded on the GDY-CuMOF nanomaterials was approximately 28.12%. AFM confirmed that the growth of CuMOF increased the height of GDY nanosheets from approximately 3.88 nm to a maximum of about 80 nm (Figures 1E and F), indicating a structural transition from two dimensions for GDY to three dimensions for GDY-CuMOF. These results strongly support the successful synthesis of GDY-CuMOF. Furthermore, the elemental composition of Cu immobilized on GDY-CuMOF was analyzed using XPS. As shown in Figure 1G, the characteristic peaks of Cu 2p3/2 and Cu 2p1/2 with binding energies (BEs) at 932.0 and 952.3 eV were observed in the Cu XPS spectrum, and the satellite peak at 942.8 eV, positioned between the two characteristic peaks, was attributed to Cu^{2+} in the paramagnetic chemical state.[29,30] This result indicates the presence of Cu with a valence state of +2 in GDY-CuMOF.

Based on this foundation, GDY-CuMOF was further loaded with DOX (GDY-CuMOF@DOX). The UV–Vis–NIR spectra of GDY-CuMOF@DOX was recorded. The primary absorption peak of DOX centred at 480–490 nm, and the GDY-CuMOF@DOX sample displayed red-shifted characteristic absorption peaks, demonstrating successful loading of DOX onto the nanomaterials (Figure 2A). Subsequently, we prepared cancer cell membranes from DU145 cells, following a previous study[31] and coated them onto the surface of GDY-CuMOF@DOX through ultrasonication to obtain the biomimetic camouflage DCM@GDY-CuMOF@DOX. A TEM image provided visual evidence that GDY-CuMOF@DOX was enveloped by a layer of membrane, confirming the successfully coating DU145 cell membrane onto the GDY-CuMOF@DOX surface (Figure 2B). The zeta potentials and particle size distributions of the various samples were investigated. As depicted in Figure 2C, the negative zeta potential of the GDY substrate was reduced from −27.8 mV to −6.14 mV after immobilization of CuMOF. The zeta potential of naked GDY-CuMOF@DOX changed from +17.0 mV to −11.4 mV after coating with DU145 cell membrane, revealing the shielding effect of the positive GDY-CuMOF@DOX by the more negative outer cancer cell membrane surface. Furthermore, the camouflage with the cell membrane also resulted in an increase in the average hydrated particle size of GDY-CuMOF@DOX from 244.0 nm to 280.5 nm (Figure 2D). Additionally, we performed sodium dodecyl sulfate-polyacrylamide gel electrophoresis (SDS-PAGE) was conducted to confirm whether the surface proteins of the DU145 cell membrane were retained on the GDY-CuMOF@DOX. As illustrated in Figure S5, DCM@GDY-CuMOF@DOX exhibited the same protein profile as that of the DU145 cell membrane, indicating that the retention of cell membrane proteins on GDY-CuMOF@DOX.

In vitro Drug Loading and Release

GDY is considered an ideal delivery vehicle for DOX aromatic anthracyclines because of its unique macroporous structure and high π-conjugation.[32,33] Therefore, we speculated that GDY-CuMOF is also capable of effectively loading DOX. Surprisingly, even at a 4:1 feeding ratio of DOX to GDY-CuMOF, we achieved a loading content as high as 77.6% and 97% entrapment efficiency for DOX, exceeded those previously reported for GDY vehicle with a 38% loading content (Figures 3A-B).[32] The excellent drug-loading capacity of GDY-CuMOF may be attributed to its coordinated three-dimensional structure, providing a higher surface area and a more porous structure. Unless otherwise stated, we used a 1:1 feeding ratio of DOX/GDY-CuMOF for subsequent experiments.

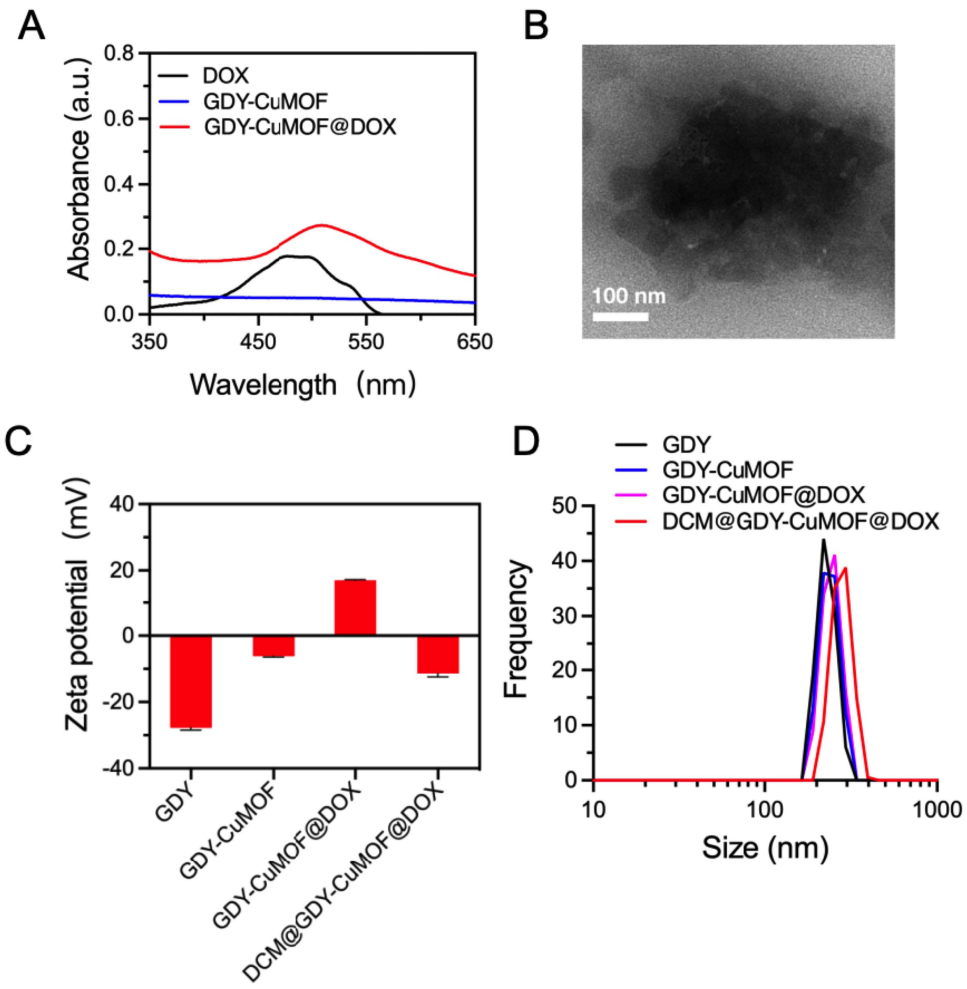

Figure 2 Characterization of DCM@GDY-CuMOF@DOX. (**A**) UV-Vis-NIR spectrum of DOX, GDY-CuMOF and GDY-CuMOF@DOX. (**B**) TEM image of DCM@GDY-CuMOF@DOX. (**C**) Zeta potentials of GDY, GDY-CuMOF, GDY-CuMOF@DOX, and DCM@GDY-CuMOF@DOX. (**D**) Size distributions of GDY, GDY-CuMOF, GDY-CuMOF@DOX, and DCM@GDY-CuMOF@DOX.

GSH is an endogenous antioxidant derived from a unique oxidative stress defense system evolved by tumor cells to circumvent the damage caused by over-expressed ROS.[34] Therefore, the intracellular concentration of GSH in tumor cells (up to 10 mM) is significantly higher than that in normal cells (approximately 2 to 4 times higher). It has been reported that copper-based organic frameworks disintegrate due to the reduction of copper from the oxidized state (Cu^{2+}) to the redox state (Cu^{+}) by GSH.[35,36] Therefore, we speculate that GDY-CuMOF@DOX also could decompose in the presence of GSH, and eventually release DOX. To confirm the potential of GDY-CuMOF@DOX to release DOX, AFM was performed to determine the structural integrity of the GDY-CuMOF after GSH treatment. As shown in Figure 3C and D, the average height of GDY-CuMOF was decreased to approximately 1.5 nm in the presence of GSH, which corresponds to that of GDY substrates, revealing the disintegration of CuMOF. Subsequently, XPS was performed to determine the valence state of Cu in GDY-CuMOF after the reaction with GSH. As illustrated in Figure 3E, the binding energies of Cu 2p3/2 and Cu 2p1/2 peaks shifted slightly from 932.0 eV and 952.3 eV to 931.6 eV and 951.5 eV, respectively. Moreover, the disappearance of the satellite peak at 942.8 eV revealed that the valence state of copper was reduced from +2 to +1 by GSH. Based on the AFM and XPS results, the DOX-releasing behavior was investigated at pH 5.0 and 7.4, in the presence or absence of GSH. As shown in Figure 3F, 58.9% and 66.4% of DOX was released in the presence of GSH after 24 h at pH 5.0, and 7.4, respectively, whereas only 11.7% to 14.8% were released in the absence of GSH. These results strongly suggest that GDY-CuMOF@DOX can disintegrate upon GSH-triggering, and correspondingly generate Cu^{+} and release DOX. In this study, the DOX-releasing behavior of DCM@GDY-CuMOF@DOX was investigated. As illustrated in Figure S6, the DOX release

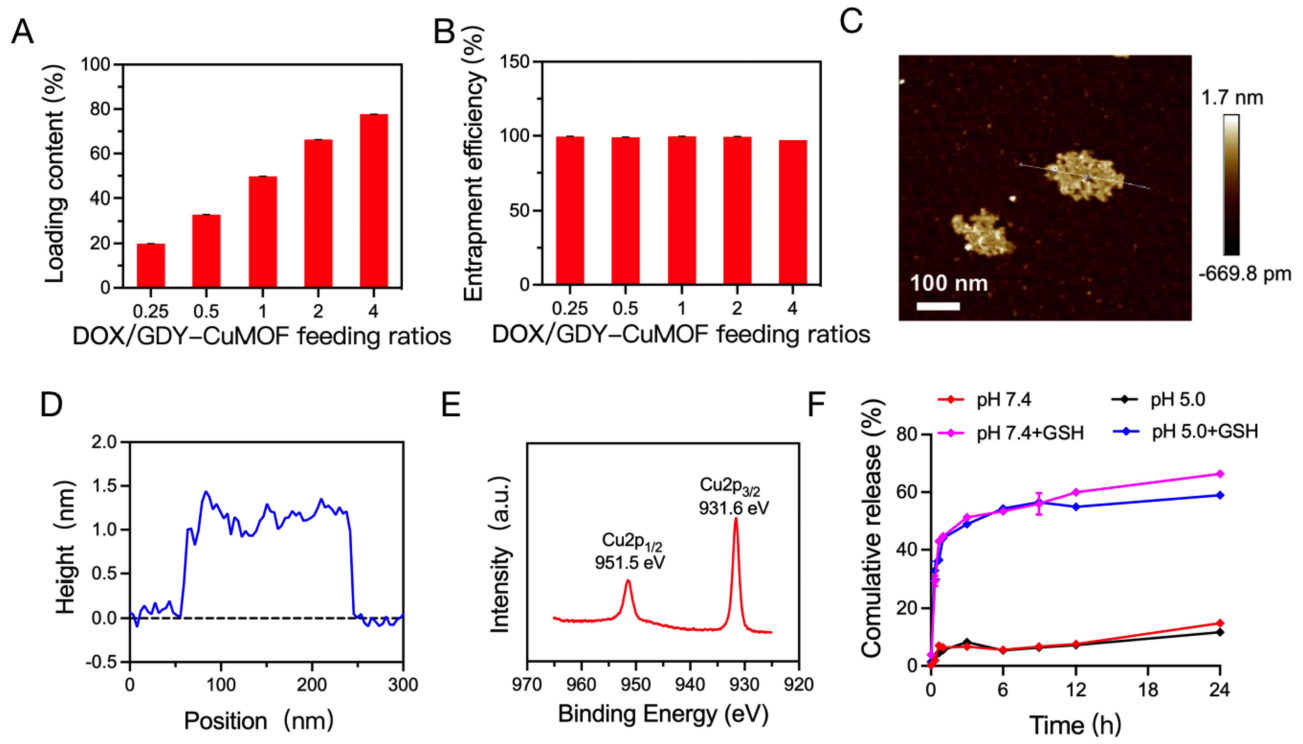

Figure 3 (**A**) Loading content and (**B**) entrapment efficiency of GDY-CuMOF@DOX at different initial DOX/GDY-CuMOF feeding ratios. (**C**) AFM image and (**D**) height of GDY-CuMOF after GSH treatment. (**E**) XPS spectrum of GDY-CuMOF after GSH treatment. (**F**) DOX released from GDY-CuMOF@DOX at pH 5.0, and 7.4, in present of GSH or not.

efficiencies of DCM@GDY-CuMOF@DOX at pH 5.0, and 7.4, were 57.8% and 61.3%, respectively, in the presence of GSH, while only 9.1% and 7.7% of that was achieved in the absence of GSH. These results confirm that the cancer cell membrane modification did not significantly affect the DOX-releasing behavior of GDY-CuMOF@DOX.

Evaluation of in vitro Antitumor Activity

The biocompatibility of GDY as a substrate and the antitumor activity of DCM@GDY-CuMOF@DOX were assessed using the CCK-8 assay. As shown in Figure S7, DU145 cells maintained more than 70% viability even after being treated with GDY at 160 μg/mL for 24 h or 48 h. This demonstrates the excellent biocompatibility of GDY as a substrate. In contrast, after 24h treatment, the viability of DU145 cells decreased significantly with increasing concentrations of free DOX, GDY-CuMOF@DOX, and DCM@GDY-CuMOF@DOX, ranging from 1.25 μg/mL to 20 μg/mL, indicating the outstanding antitumor activity of the all three (Figure 4A). Moreover, it can be observed that the antitumour activity of all three was further enhanced by extending the incubation time (Figure 4B). In general, drug delivery vehicles are taken up by cells through endocytosis, with a portion of the drug being gradually released within the cell over time, whereas free drugs can penetrate directly into the cells through passive diffusion. Thus, free DOX generally exhibits a more pronounced antitumor efficacy in vitro. Additionally, the incomplete release of DOX from DCM@GDY-CuMOF@DOX contributed to the higher antitumor efficacy of free DOX compared to DCM@GDY-CuMOF@DOX. Positively charged nanoparticles typically exhibited poor plasma stability, and rapid clearance from blood circulation, and can induce more severe cytotoxicity than negatively charged variants of similar sizes.[37] Therefore, GDY-CuMOF@DOX without modifications showed a considerably lower antitumor efficiency than DCM@GDY-CuMOF@DOX at all doses. After DCM@GDY-CuMOF@DOX treatment for 24 h and 48 h, even at low concentrations of 20 μg/mL, 60.5% and 85.7% of the DU145 cells were killed, demonstrating the excellent antitumor activity of DCM@GDY-CuMOF@DOX. Furthermore, GDY-CuMOF exhibited negligible cytotoxicity. The inhibitory effect of DCM@GDY-CuMOF@DOX on PC3 cells was also investigated using the CCK-8 assay. After treatment with DCM@GDY-CuMOF@DOX for 24 h and

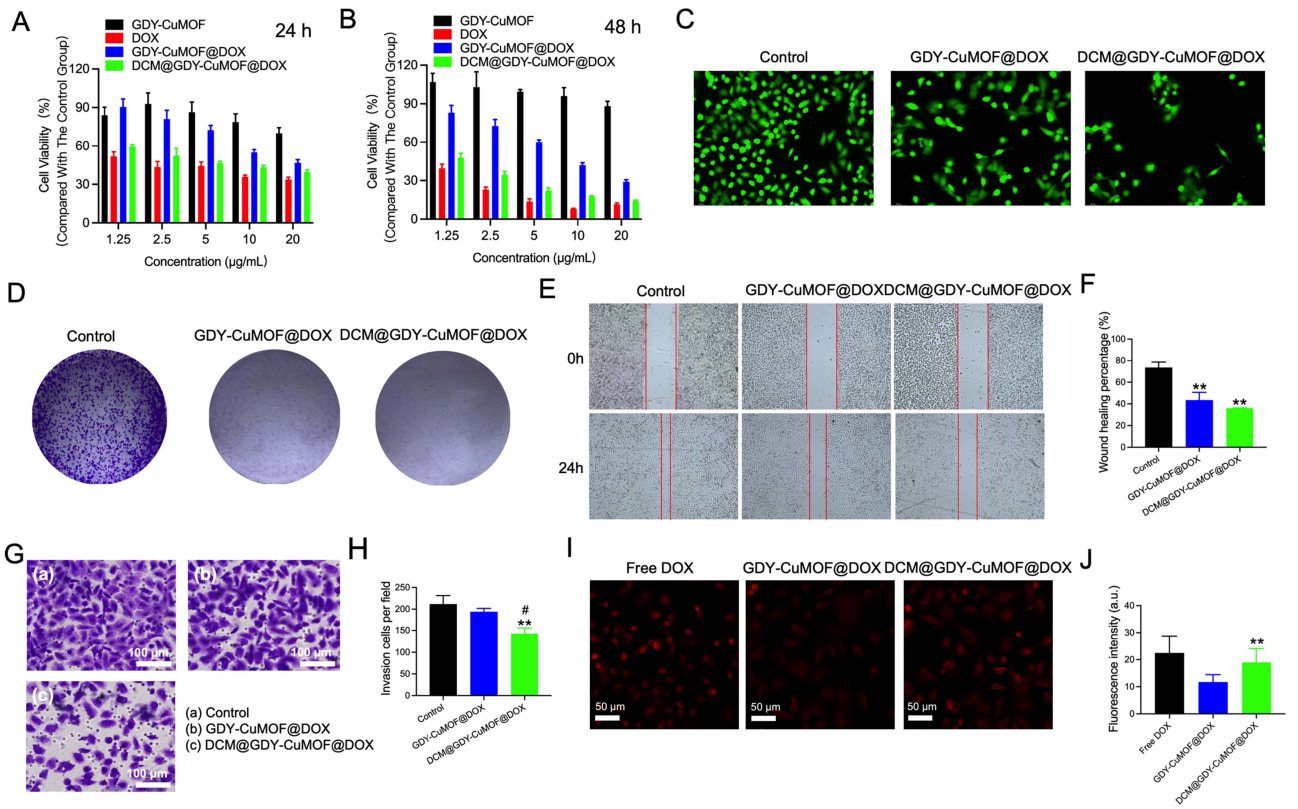

Figure 4 Antitumor effects of various nanomaterials. (**A-B**) The cell viability of DU145 cells treated with various sample (GDY-CuMOF, free DOX, GDY-CuMOF@DOX, and DCM@GDY-CuMOF@DOX) for 24 h and 48 h determined by CCK-8 assay. (**C**) The live cell staining of DU145 cells incubated with PBS, GDY-CuMOF@DOX and DCM@GDY-CuMOF@DOX. (**D**) The clonogenic assay of DU145 cells treated with PBS, GDY-CuMOF@DOX and DCM@GDY-CuMOF@DOX. (**E**) The wound healing assay of DU145 cells treated with PBS, GDY-CuMOF@DOX, and DCM@GDY-CuMOF@DOX for 24 h. The red lines indicate the cell boundaries. (**F**) The wound healing rate analysis in Figure 4E (n = 3). (**G**) The invasion assay of DU145 cells treated with PBS, GDY-CuMOF@DOX and DCM@GDY-CuMOF@DOX. (**H**) Statistical analysis of invasive cells from Figure 4G (n = 3). (**I**) Fluorescence images of DU145 cells treated with free DOX, GDY-CuMOF@DOX, and DCM@GDY-CuMOF@DOX (equivalent DOX concentration of 10 μg/mL). The red fluorescence represents intracellular DOX. (**J**) The average fluorescence intensity quantified from Figure 4I The label ** indicates $p < 0.01$ compared with the control group, and the label # indicates $p < 0.05$ compared with the GDY-CuMOF@DOX group.

48 h, PC3 cells at a concentration of 20 μg/mL maintained 78.9% and 59.6% viability, respectively (Figure S8). Interestingly, in contrast to DU145 cells, the inhibitory effect of DCM@GDY-CuMOF@DOX on PC3 cells was mainly enhanced by prolonging the treatment time rather than by increasing the concentration. Such a result may be due to the different uptake efficiency of the nanoplatforms by the heterologous cells.

Subsequently, live cell staining was performed to evaluate antitumor effect of GDY-CuMOF@DOX and DCM@GDY-CuMOF@DOX. As shown in Figure 4C, the strong green fluorescence can be clearly observed in the untreated cells. In contrast, both GDY-CuMOF@DOX- and DCM@GDY-CuMOF@DOX-treated cells showed a clear decrease in green fluorescence, while the cells treated with DCM@GDY-CuMOF@DOX showed the most significant decrease in fluorescence, indicating the excellent effect of DCM@GDY-CuMOF@DOX to induce cell death. Next, a clonogenic assay was conducted to investigate the effects of GDY-CuMOF@DOX and DCM@GDY-CuMOF@DOX on the replication capacity of DU145 cells. As shown in Figure 4D and Figure S9, it was challenging to detect colonies in the samples after DCM@GDY-CuMOF@DOX treatment. This indicates that DCM@GDY-CuMOF@DOX was more effective than GDY-CuMOF@DOX in suppressing the proliferative capacity of PCa cells. Similarly, wound healing assay and transwell invasion assays further validated that the migratory and invasive ability of DU145 cells were significantly inhibited by DCM@GDY-CuMOF@DOX (Figures 4E-H). Furthermore, it can be observed that the inhibitory effect of GDY-CuMOF@DOX was enhanced after the cancer cell membrane modification, which is in good agreement with the clonogenic assay results.

Because DOX possesses fluorescent properties, it can be serve as a probe for tracking the intracellular localization of nanomaterials. To gain insights into the enhanced antitumor activity of DCM@GDY-CuMOF@DOX in comparison to

that of GDY-CuMOF@DOX, the presence of DOX in DU145 cells treated with free DOX, GDY-CuMOF@DOX, or DCM@GDY-CuMOF@DOX was visualized using a LSCM. As depicted in Figures 4I-J, it is evident that the cells treated with GDY-CuMOF@DOX exhibited a weaker red fluorescence signal compared to free DOX. In contrast, DCM@GDY-CuMOF@DOX significantly increased the intracellular fluorescence intensity, indicating that the DU145 cell membrane coating promoted the uptake of the nanoplatform by DU145 cells. Moreover, flow cytometry was used to quantify the DOX fluorescence in DU145 cells after treatment with PBS, Free DOX, GDY-CuMOF@DOX, or DCM@GDY-CuMOF@DOX. As shown in Figure S10, free DOX-treated cells showed the strongest fluorescence intensity because DOX can penetrate directly into the cells by passive diffusion. Compared to GDY-CuMOF@DOX group, DCM@GDY-CuMOF@DOX group showed enhanced fluorescence intensity. This indicates that DCM@GDY-CuMOF@DOX can be taken up more efficiently by DU145 cells. It has been reported that adhesion molecules (eg adhesion proteins and integrins) on the surface of cancer cell membranes can confer homologous recognition and homing properties to nanomaterials.[38–40] This result confirms that the improved antitumor effect of the nanomaterials can be attributed to the homotypic targeting ability of DCM@GDY-CuMOF@DOX.

Antitumor Mechanism of DCM@GDY-CuMOF@DOX

As expected, DCM@GDY-CuMOF@DOX exhibited superior antitumor activity against DU145 cells. To further elucidate the specific antitumor mechanism of DCM@GDY-CuMOF@DOX, we measured endocellular ROS levels in DU145 cells treated with different samples using a ROS probe, DCFH-DA. As shown in Figures 5A-B, an intense green

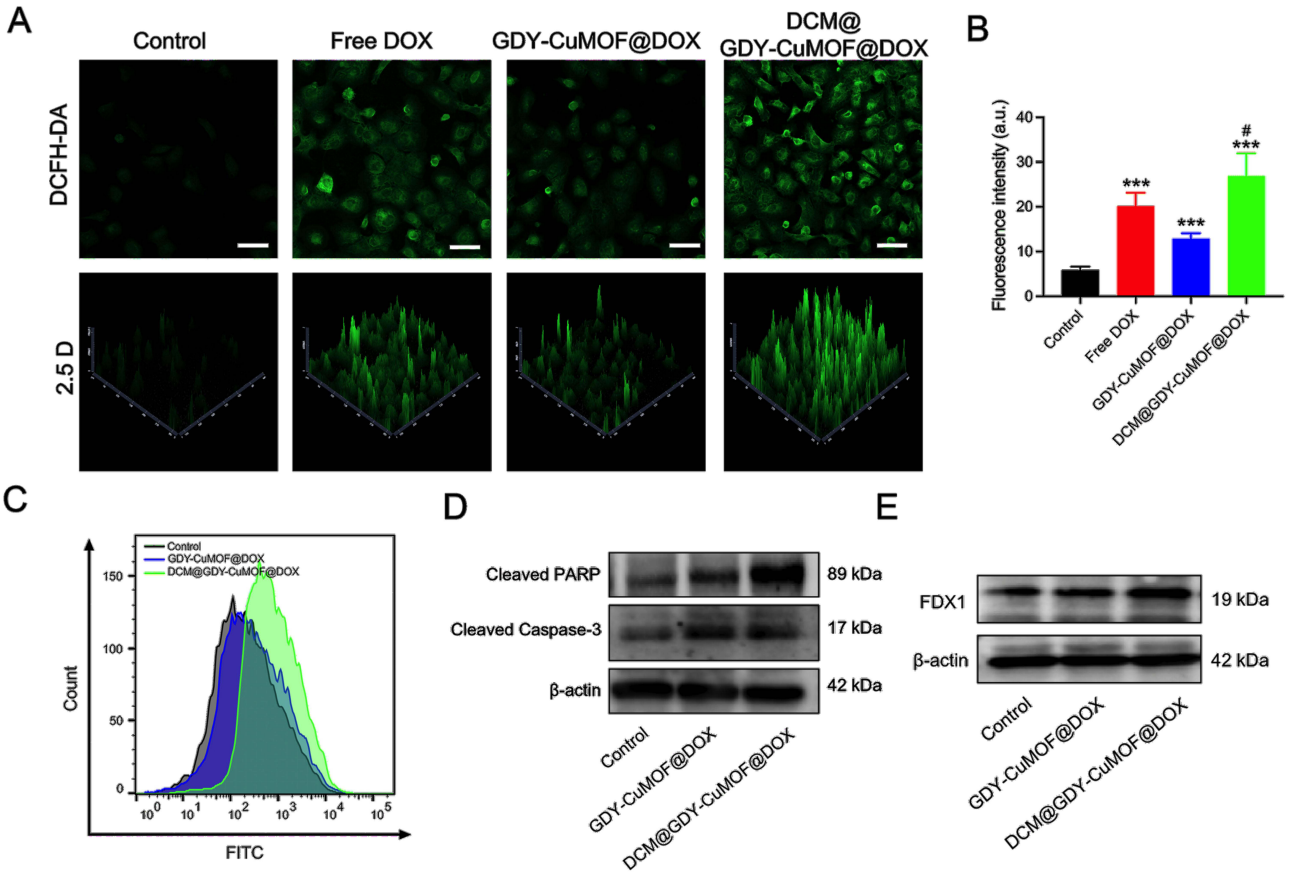

Figure 5 Antitumor mechanism of DCM@GDY-CuMOF@DOX. (**A**) Fluorescence images of DU145 cells treated with free DOX, GDY-CuMOF@DOX, and DCM@GDY-CuMOF@DOX (equivalent DOX concentration of 10 μg/mL). The green fluorescence indicates intracellular ROS. (**B**) The average fluorescence intensity quantified from Figure 5A. The label *** indicates $p < 0.001$ compared with the control group, and the label # indicates $p < 0.05$ compared with the GDY-CuMOF@DOX group. (**C**) The flow cytometry quantitative analysis of ROS level of DU145 cells after 24 h treatment with PBS, GDY-CuMOF@DOX (20 μg/mL), and DCM@GDY-CuMOF@DOX (20 μg/mL). (**D**) The expression level of cleaved PARP, cleaved Caspase-3 protein of DU145 cells treated with GDY-CuMOF@DOX or DCM@GDY-CuMOF@DOX at 20 μg/mL for 24 h. (**E**) The expression level of FDX1 protein of DU145 cells treated with GDY-CuMOF@DOX or DCM@GDY-CuMOF@DOX at 20 μg/mL for 24 h.

fluorescence signal was observed in the free DOX group, demonstrating that DOX induced a large amount of ROS (H_2O_2) in the cells. It has been reported that DOX is a potent pro-oxidant, which can elevate the H_2O_2 level in tumor cells. Mechanistically, DOX first undergoes conversion to semiquinone, which in turn reduces oxygen to superoxide and generates H_2O_2.[41] A slightly weaker green fluorescence signal than that of the free DOX group can be observed in the cells treated with GDY-CuMOF@DOX. GDY-CuMOF@DOX was shown to disintegrate in the presence of GSH, resulting in the production of reductive Cu^+ and the release of DOX. Thus, in our study, when DU145 cells were treated with GDY-CuMOF@DOX, DOX was first released from GDY-CuMOF@DOX by GSH, triggering an increase in the concentration of intracellular H_2O_2, which was subsequently converted to more toxic ROS (·OH) catalyzed by Cu^+ ions via a Fenton-like reaction. Notably, the DCM@GDY-CuMOF@DOX group showed a stronger fluorescence signal than the GDY-CuMOF@DOX group, confirming the higher ROS production efficiency of the DCM@GDY-CuMOF@DOX group. Moreover, flow cytometry also suggested that DCM@GDY-CuMOF@DOX induced more pronounced ROS production than GDY-CuMOF@DOX (Figure 5C). These results were attributed to the fact that the coating of cancer cell membranes promoted the uptake of GDY-CuMOF@DOX by homotypic cells.

Next, the apoptotic pathways triggered by GDY-CuMOF@DOX and/or DCM@GDY-CuMOF@DOX were investigated through Western blotting. As illustrated in Figure 5D, the expression levels of cleaved poly(ADP-ribose) polymerase (PARP), and cleaved Caspase-3 protein were increased significantly in DU145 cells after treatment with GDY-CuMOF@DOX or DCM@GDY-CuMOF@DOX. It has been reported that ROS induces apoptosis by causing oxidative DNA damage and mitochondrial dysfunction and further activating PARP cleavage and Caspase cascade.[42] These results strongly suggested that apoptosis triggered by GDY-CuMOF@DOX or DCM@GDY-CuMOF@DOX is associated with excessive ROS generation. Additionally, since cell death induced by cuproptosis involves the destruction of specific metabolic enzymes in the mitochondria, we also investigated the expression of related protein in DU145 cells. Incubation with either GDY-CuMOF@DOX or DCM@GDY-CuMOF@DOX remarkably increased the expression of Ferredoxin1 (FDX1) in DU145 cells (Figure 5E and Figure S11). FDX1 is reportedly a key regulator of protein lipoylation in the mitochondria, and is responsible for reducing Cu^{2+} to its more lethal form, Cu^+. This result indicates that these copper-containing nanomaterials also induced cell death through cuproptosis.

In vivo Antitumor Therapy

Encouraged by the results of the in vitro experiments, we proceeded to evaluate the in vivo antitumor activity of DCM@GDY-CuMOF@DOX in BALB/c nude mice bearing DU145 tumors. The mice were randomly divided into four groups, each consisting of four mice, and were intravenously injected five times at days 0, 3, 6, 9, and 12 with different substances: PBS (negative control), DOX (5 mg/kg, positive control), GDY-CuMOF@DOX (5 mg/kg), DCM@GDY-CuMOF@DOX (5 mg/kg). As depicted in Figure 6A, rapid tumor growth was observed in the mice treated with intravenous PBS and GDY-CuMOF@DOX. As expected, DCM@GDY-CuMOF@DOX significantly inhibited tumor growth, with effects comparable to those in the positive control group. The inhibition rate of tumor, determined by tumor weight, was as high as 47.9% in the DCM@GDY-CuMOF@DOX treatment group and 4.6% in the GDY-CuMOF@DOX treatment group (Figure 6B). During the treatment period, the mice treated with DCM@GDY-CuMOF@DOX showed no difference from the control group in terms of body weight and survival rate (Figure 6C and Figure S12). In contrast, mice treated with free DOX showed a trend toward decreased body weight.

To gain insight into the improved in vivo antitumor effect of DCM@GDY-CuMOF@DOX, we conducted ICP-MS to detect the Cu content in the tumor tissues and the major organs of the PBS, GDY-CuMOF@DOX and DCM@GDY-CuMOF@DOX treatment groups. As shown in Figure S13, the tumor tissues of the DCM@GDY-CuMOF@DOX treatment group exhibited higher Cu content, suggesting that DCM@GDY-CuMOF@DOX can accumulate in the tumor tissues more efficiently. The mice treated with GDY-CuMOF@DOX showed different degrees of Cu accumulation in major organs, while those treated with DCM@GDY-CuMOF@DOX showed no difference in Cu content in major organs compared with the control group, suggesting that the biomimetic camouflage of the nanoplatforms reduced their accumulation in major organs (Figure S14). Based on the above results, the increased antitumor efficiency of DCM@GDY-CuMOF@DOX compared with that of GDY-CuMOF@DOX may be attributed to the excellent performance of DCM@GDY-CuMOF@DOX in homotypic tumor targeting. Furthermore, we performed the histological

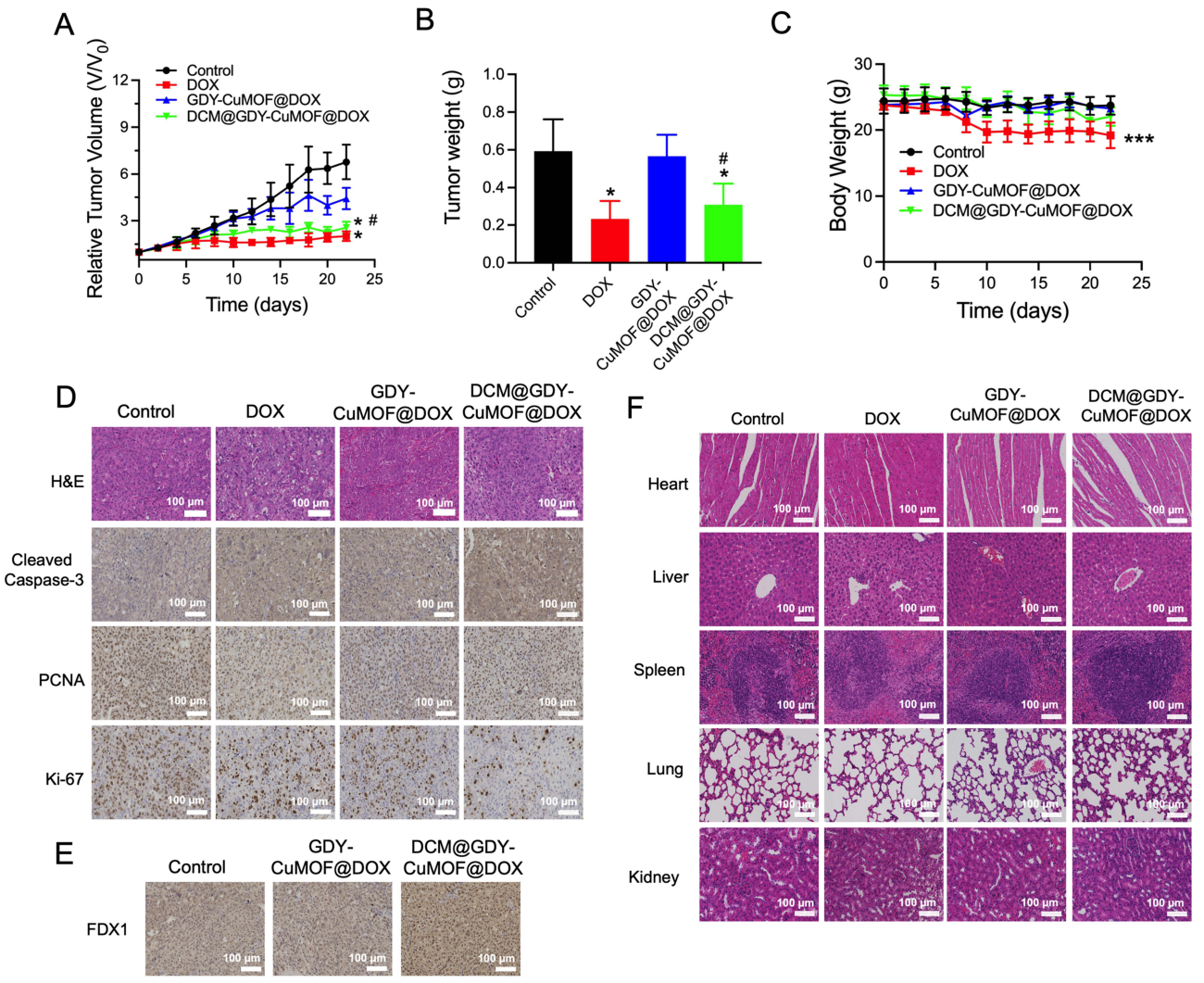

Figure 6 The antitumor efficacy of DCM@GDY-CuMOF@DOX in vivo. (**A**) Changes in the relative volume of tumors in the different treatment groups over the treatment period. (**B**) Tumor weight in different treatment groups. The label * indicates $p < 0.05$ compared with the control group, and the label # indicates $p < 0.05$ compared with the GDY-CuMOF@DOX group. (**C**) changes in body weight of mice treated with different samples during the treatment period. The label *** indicate $p < 0.001$ compared with the control group. (**D**) H&E staining and immunohistochemical analysis images (cleaved Caspase-3, PCNA and Ki-67) of tumor tissue from different treatment groups. (**E**) immunohistochemical analysis images (FDX1) of tumor tissue from GDY-CuMOF@DOX and DCM@GDY-CuMOF@DOX groups. (**F**) H&E staining of heart, liver, spleen, lung and kidney from different treatment groups.

evaluation of the harvested tumor sections to investigate the therapeutic effects of DCM@GDY-CuMOF@DOX using H&E staining and immunohistochemical analysis (Figure 6D). In the DCM@GDY-CuMOF@DOX treatment group, obvious apoptosis and extensive necrosis were observed in H&E staining of tumour tissue compared to the control group, indicating that DCM@GDY-CuMOF@DOX could effectively induce apoptosis and promote necrosis of cancer cells to suppress tumour growth. Moreover, the immunohistochemical analysis revealed that the expression level of cleaved Caspase-3 was upregulated in the DCM@GDY-CuMOF@DOX treatment group, further indicating ROS-induced apoptosis. In comparison, tumors treated with DCM@GDY-CuMOF@DOX exhibited downregulation by PCNA and Ki-67 levels, indicating the suppression of tumor cell proliferation. Notably, the expression level of FDX1 was significantly elevated in the DCM@GDY-CuMOF@DOX treatment group, suggesting its involvement of cuproptosis in the inhibition of tumor cell growth (Figure 6E). These results were consistent with previous findings that DCM@GDY-CuMOF@DOX kills tumor cells by inducing ROS and mediating cuproptosis.

The biocompatibility of the nanoplatform was also evaluated. As shown in Figure 6F, DCM@GDY-CuMOF@DOX did not cause significant damage to the major organs, including the heart, liver, spleen, lungs and kidneys. The hemolysis effect of DCM@GDY-CuMOF@DOX was evaluated by hemolysis experiment (Figure S15). Compared to the water group, only slight

hemolysis was observed in the DCM@GDY-CuMOF@DOX group, indicating that the nanoplatforms have good blood compatibility. The serum biochemical indicators in the DCM@GDY-CuMOF@DOX group also showed no significant differences compared to those in the control group, revealing the good biocompatibility and biosafety of DCM@GDY-CuMOF@DOX (Figure S16). In contrast, mice treated with free DOX showed marked tubular degeneration and necrosis in the renal tissue, and abnormalities in serum biochemical indicators such as AST and LDH1. This suggests that DOX cause severe systemic toxicity in mice.

Conclusion

In summary, we developed a biomimetic GSH-responsive nanoplatform with the tumor-targeting ability for PCa therapy. Modification of tumor cell membranes endows the nanoplatform with homotypic targeting capabilities. In the GSH environment, Cu^{+} and DOX are released from the nanoplatforms, increasing the intensity of the Fenton-like reaction and stimulating the generation of cytotoxic ROS from endogenous H_2O_2, resulting in a highly effective chemodynamic therapy. As expected, DCM@GDY-CuMOF@DOX effectively kills tumor cells and inhibits tumor cell migration and invasion in vitro by inducing ROS generation and mediating cuproptosis. More importantly, DCM@GDY-CuMOF@DOX inhibits tumor growth in vivo without causing significant systemic toxicity. Therefore, DCM@GDY-CuMOF@DOX may represent a promising nanoplatform for integrating tumor targeting, drug-responsive release, and combination therapy for PCa treatment.

Acknowledgments

The work was supported by National Natural Science Foundation of China (No. 82072813), Guangdong Basic and Applied Basic Research Foundation (No. 2020A1515110640), The Science and Technology Development Fund, Macau SAR (No. 0090/2022/A), Guangdong Key Laboratory of Clinical Molecular Medicine and Diagnostics (No. SYS001), Science and Technology Projects in Guangzhou (No. 2023A03J0965), Youth Medical Innovation and Practice Research Program of Guangzhou (No. 2023QNYXYB012).

Disclosure

The authors declare no conflict of interest.

References

1. Siegel RL, Miller KD, Jemal A. Cancer statistics, 2018. *Ca a Cancer J Clinicians*. 2018;68(1):7–30. doi:10.3322/caac.21442
2. Teo MY, Rathkopf DE, Kantoff P. Treatment of advanced prostate cancer. *Annual Review of Medicine*. 2019;70(1):479–499. doi:10.1146/annurev-med-051517-011947
3. Sartor O. Curing more prostate cancer: thinking through the options. *J clin oncol*. 2018;36(15):1466–1468. doi:10.1200/jco.2018.78.4835
4. Kamba T. Bone-targeted treatment in CRPC management. *Hormo Therapy Castr Res Pros Cancer*. 317–325. 10.1007/978-981-10-7013-6_32
5. Zhao H, Freedland S. Enzalutamide treatment for the whole spectrum of CRPC. *Nat Rev Urol*. 2018;15(11):663–665. doi:10.1038/s41585-018-0090-1
6. Hadaschik B, Hellmis E. Therapie des nicht-Fernmetastasierten CRPC. *Der Urologe*. 2021;60(6):753–759. doi:10.1007/s00120-021-01473-0
7. Rae TD, Schmidt PJ, Pufahl RA, Culotta VC V, O' Halloran T. Undetectable intracellular free copper: the requirement of a copper chaperone for superoxide dismutase. *Science*. 1999;284(5415):805–808. doi:10.1126/science.284.5415.805
8. B-E K, Nevitt T, Dj T. Mechanisms for copper acquisition, distribution and Regulation. *Nature Chem Bio*. 2008;4(3):176–185. doi:10.1038/nchembio.72
9. Tchounwou PB, Yedjou CG, Patlolla AK, Sutton DJ. Heavy metal toxicity and the environment. *Experientia Supplementum*. 2012;101:133–164. doi:10.1007/978-3-7643-8340-4_6
10. Jomova K, Valko M. Advances in metal-induced oxidative stress and human disease. *Toxicology*. 2011;283(2–3):65–87. doi:10.1016/j.tox.2011.03.001
11. Tsvetkov P, Coy S, Petrova B, et al. Copper induces cell death by targeting lipoylated TCA cycle proteins. *Science*. 2022;375(6586):1254–1261. doi:10.1126/science.abf0529
12. S-R L, L-L B, Cai L. Cuproptosis: lipoylated TCA cycle proteins-mediated novel Cell Death pathway. *Signal Trans Targe Thera*. 2022;7(1). doi:10.1038/s41392-022-01014-x
13. Cardoso HJ, Carvalho TM, Fonseca LR, Figueira MI, Vaz CV, Socorro S. Revisiting prostate cancer metabolism: from metabolites to disease and therapy. *Med Res Rev*. 2020;41(3):1499–1538. doi:10.1002/med.21766
14. Chen H, Li X, Huo M, et al. Tumor-responsive copper-activated disulfiram for synergetic nanocatalytic tumor therapy. *Nano Res*. 2020;14(1):205–211. doi:10.1007/s12274-020-3069-1
15. Oliveri V. Biomedical applications of copper ionophores. *Coord Chem Rev*. 2020;422:213474. doi:10.1016/j.ccr.2020.213474
16. Banci L, Bertini I, Ciofi-Baffoni S, Kozyreva T, Zovo K, Palumaa P. Affinity gradients drive copper to cellular destinations. *Nature*. 2010;465(7298):645–648. doi:10.1038/nature09018
17. Geim AK, Novoselov KS. The rise of graphene. *Nature Mater*. 2007;6(3):183–191. doi:10.1038/nmat1849

18. Li Y, Xu L, Liu H, Li Y. Graphdiyne and graphyne: from theoretical predictions to practical construction. *Chem Soc Rev*. 2014;43(8):2572. doi:10.1039/c3cs60388a
19. Huang C, Li Y, Wang N, et al. Progress in research into 2D graphdiyne-based materials. *Chem Rev*. 2018;118(16):7744–7803. doi:10.1021/acs.chemrev.8b00288
20. Zhang Y, Xie W, Lin J, et al. Untargeted metabolomics to analyze alterations in two-dimensional graphdiyne–copper nanocomposite on the metabolic reprogramming of prostate cancer. *2D Mater*. 2022;10(1):015011. doi:10.1088/2053-1583/ac9e67
21. Huang Z, Chen G, Deng F, Li Y. Nanostructured graphdiyne: synthesis and biomedical applications. *Int j Nanomed*. 2022;17:6467–6490. doi:10.2147/IJN.S383707
22. Šimůnek T, Štěrba M, Popelová O, Adamcová M, Hrdina R, Geršl V. Anthracycline-induced cardiotoxicity: overview of studies examining the roles of oxidative stress and Free Cellular Iron. *Pharmacol Rep*. 2009;61(1):154–171. doi:10.1016/s1734-1140(09)70018-0
23. Menna P, Recalcati S, Cairo G, Minotti G. An introduction to the metabolic determinants of anthracycline cardiotoxicity. *Cardiovasc Toxicol*. 2007;7(2):80–85. doi:10.1007/s12012-007-0011-7
24. Lin J, Yang H, Zhang Y, et al. Ferrocene-based polymeric nanoparticles carrying doxorubicin for oncotherapeutic combination of chemotherapy and ferroptosis. *Small*. 2022;19(2). doi:10.1002/smll.202205024
25. Brillas E, Baños MA, Camps S, et al. Catalytic effect of fe2+, cu2+and UVA light on the electrochemical degradation of nitrobenzene using an oxygen-diffusion cathode. *New J Chem*. 2004;28(2):314–322. doi:10.1039/b312445b
26. Soltani T, Lee B-K. Enhanced formation of sulfate radicals by metal-doped BIFEO3 under visible light for improving photo-fenton catalytic degradation of 2-chlorophenol. *Chem Eng J*. 2017;313:1258–1268. doi:10.1016/j.cej.2016.11.016
27. Li G, Li Y, Liu H, Guo Y, Li Y, Zhu D. Architecture of graphdiyne nanoscale films. *Chem Commun*. 2010;46(19):3256. doi:10.1039/b922733d
28. Xie M, Deng T, Li J, Shen H. The camouflage of graphene oxide by red blood cell membrane with high dispersibility for cancer chemotherapy. *J Colloid Interface Sci*. 2021;591:290–299. doi:10.1016/j.jcis.2021.01.088
29. Zhang J, Yu J, Zhang Y, Li Q, Gong JR. Visible light photocatalytic H2-production activity of CUS/zns porous nanosheets based on photoinduced interfacial charge transfer. *Nano Lett*. 2011;11(11):4774–4779. doi:10.1021/nl202587b
30. Koski KJ, Cha JJ, Reed BW, Wessells CD, Kong D, Cui Y. Cheminform abstract: high-Density Chemical Intercalation of zero-valent copper into bi2se3 nanoribbons. *ChemInform*. 2012;43(34). doi:10.1002/chin.201234008
31. Dehaini D, Wei X, Fang RH, et al. Erythrocyte–platelet hybrid membrane coating for enhanced nanoparticle functionalization. *Adv Mater*. 2017;29(16). doi:10.1002/adma.201606209
32. Jin J, Guo M, Liu J, et al. Graphdiyne nanosheet-based drug delivery platform for photothermal/chemotherapy combination treatment of cancer. *ACS Appl Mater Interfaces*. 2018;10(10):8436–8442. doi:10.1021/acsami.7b17219
33. Li S, Chen Y, Liu H, et al. Graphdiyne materials as nanotransducer for in vivo photoacoustic imaging and photothermal therapy of tumor. *Chem Mater*. 2017;29(14):6087–6094. doi:10.1021/acs.chemmater.7b01965
34. Zhu J, Wang X, Su Y, et al. Multifunctional nanolocks with GSH as the key for synergistic ferroptosis and anti-chemotherapeutic resistance. *Biomaterials*. 2022;288:121704. doi:10.1016/j.biomaterials.2022.121704
35. Du J, Chen G, Yuan X, Yuan J, Li L. Multi-stimuli responsive cu-mofs@keratin drug delivery system for Chemodynamic therapy. *Front Bioeng Biotechnol*. 2023;11. doi:10.3389/fbioe.2023.1125348
36. Zheng H, Zhang Y, Liu L, et al. One-pot synthesis of metal–organic frameworks with encapsulated target molecules and their applications for controlled drug delivery. *J Am Chem Soc*. 2016;138(3):962–968. doi:10.1021/jacs.5b11720
37. Souris JS, Lee C-H, Cheng S-H, et al. Surface charge-mediated rapid hepatobiliary excretion of mesoporous silica nanoparticles. *Biomaterials*. 2010;31(21):5564–5574. doi:10.1016/j.biomaterials.2010.03.048
38. Chi S, Zhang L, Cheng H, et al. Biomimetic nanocomposites camouflaged with hybrid cell membranes for accurate therapy of early-stage glioma. *Angew Chem*. 2023;135(29):e202304419. doi:10.1002/anie.202304419
39. Li J, Zhang J, Gao Y, et al. Targeted siRNA delivery by bioinspired cancer cell membrane-coated nanoparticles with enhanced anti-cancer immunity. *Int j Nanomed*. 2023;18:5961–5982. doi:10.2147/IJN.S429036
40. Wu Y, Zhu R, Zhou M, et al. Homologous cancer cell membrane-camouflaged nanoparticles target drug delivery and enhance the chemotherapy efficacy of hepatocellular carcinoma. *Cancer Lett*. 2023;558:216106. doi:10.1016/j.canlet.2023.216106
41. Czepas J, Koceva-Chyła A, Gwoździński K, Jóźwiak Z. Different effectiveness of piperidine nitroxides against oxidative stress induced by doxorubicin and hydrogen peroxide. *Cell Biol Toxicol*. 2007;24(1):101–112. doi:10.1007/s10565-007-9020-3
42. Tan P, Cai H, Wei Q, et al. Enhanced chemo-photodynamic therapy of an enzyme-responsive prodrug in bladder cancer patient-derived xenograft models. *Biomaterials*. 2021;277:121061. doi:10.1016/j.biomaterials.2021.121061